American Mineralogist, Volume 74, pages 610–619, 1989

Iron distribution in staurolite at room and low temperatures

VELINDA D. ALEXANDER
Department of Geology, Brigham Young University, Provo, Utah 84602, U.S.A.

ABSTRACT

X-ray diffraction and Mössbauer spectroscopy at room and liquid-N_2 temperatures have been used to examine the Fe distribution in a staurolite with an approximate composition of

$$Fe_{2.33}Mg_{0.94}Zn_{0.65}Ti_{0.09}Mn_{0.08}Al_{18.10}Si_{7.26}O_{43.8}(OH)_{4.2}.$$

The space group is $C2/m$, and lattice parameters at room and low temperatures, respectively, are a = 7.865(2) and 7.871(2) Å, b = 16.580(4) and 16.587(5) Å, c = 5.668(3) and 5.661(3) Å, and β = 90.38(5)° and 90.39(7)°. Optical properties measured for this staurolite are α = 1.738(2), β = 1.743(2), γ = 1.747(2), and $2V_X$ = 89.5(7)°. The Mössbauer spectra are fit to four doublets, resulting in χ^2 values of 1.2 and 1.3 for the room- and low-temperature spectra, respectively. The room- and low-temperature structure refinements resulted in R values of 0.031 and 0.032, respectively.

The following distribution of Fe is derived solely from structure-refinement results: 92% in $^{[4]}$**Fe**, 6% in $^{[6]}$**Al(3)**, and 2% in $^{[6]}$**U**. Mössbauer spectra indicate that 5–10% of the Fe is trivalent. The three largest Mössbauer doublets are attributed to Fe^{2+} in energetically nonequivalent $^{[4]}$**Fe** sites. Positional disorder at the **Fe** site is attributed to variations in the crystal-field energy at the **Fe** site. Intensities of the Mössbauer doublets and of the electron-density peaks at the **Fe** site exhibit no definite temperature dependence.

INTRODUCTION

The crystal structure of staurolite has been a subject of study for nearly 50 years. Various investigators, using X-ray–diffraction or neutron-diffraction techniques, have determined locations and approximate occupancies for all sites and approximate site distributions for most cations (Náray-Szabó, 1929; Náray-Szabó and Sasvári, 1958; Hanisch, 1966; Smith, 1968; Takéuchi et al., 1972; Tagai and Joswig, 1985; Bringhurst and Griffen, 1986). The structure of staurolite consists of layers of kyanite-like structure and composition alternating with monolayers, one atom thick, containing sites occupied mostly by Fe, Al, and Mg (Smith, 1968). The monolayers also accommodate elements such as Mn, Zn, Ti, and Co (Smith, 1968; Griffen, 1981; Ward, 1984b; Bringhurst and Griffen, 1986). The tetrahedral **Si** site and the octahedral **Al(1A)**, **Al(1B)**, and **Al(2)** sites are located in the kyanite layer and are all nearly fully occupied. (Site names are in bold-face type to distinguish them from the symbols for chemical elements.) The tetrahedral **Fe** site and the partially occupied octahedral **Al(3A)**, **Al(3B)**, **U(1)**, and **U(2)** sites are located in the monolayer (Fig. 1). The proton sites, **P(1A)** and **P(1B)**, are located near **O(1A)** and **O(1B)** in the faces of the **Al(3A)** and **Al(3B)** octahedra (Takéuchi et al., 1972).

In spite of all the effort that has been expended on this mineral, its crystal chemistry is still not completely understood. One unresolved question centers around the distribution of Fe in the structure. Mössbauer spectroscopy has proved invaluable in determining valence states and coordination numbers of Fe atoms in the crystal structures of many minerals and has been applied to staurolite several times. The first Mössbauer spectrum of staurolite was reported by De Coster et al. (1963). Better results were obtained later by Bancroft et al. (1967); they resolved the spectrum into two doublets and concluded that most Fe in staurolite is divalent. On the basis of the Mössbauer parameters of the two doublets in the spectrum, they assigned the outer doublet to tetrahedrally coordinated Fe and the inner doublet to octahedrally coordinated Fe. This interpretation was accepted by some later workers (Smith, 1968; Takéuchi et al., 1972; Phillips and Griffen, 1986) who partitioned 20–25% of the Fe into sites other than the tetrahedral **Fe** site on the basis of the peak intensities of Mössbauer spectra taken from their particular staurolite specimens. In a Mössbauer study of single crystals of staurolite at different temperatures, Regnard (1976) fit his spectra with three Fe^{2+} doublets and one (small) Fe^{3+} doublet. He also followed the Bancroft et al. (1967) interpretation by assigning the two inner doublets to octahedrally coordinated Fe and the outer doublet to tetrahedrally coordinated Fe.

Other workers have proposed different interpretations, however. Dowty (1972) first noted the large temperature dependence of the inner doublet (see Dowty's Fig. 2) and suggested that the Fe may be partitioned among two or more subsites within the **Fe** site and may not be in the octahedral sites at all. An electron-density difference map of the **Fe** site published by Smith (1968) shows as many

0003–004X/89/0506–0610$02.00

as four possible subsites within the **Fe** site and supports Dowty's idea, although Smith followed the Bancroft et al. (1967) interpretation. Scorzelli et al. (1976) attributed the temperature dependence of the inner doublet to electron exchange between Fe^{2+} and electrophilic anion vacancies necessitated by substitution of Fe^{2+} for Al^{3+} in the octahedral sites. Dickson and Smith (1976) investigated the effects of low temperature on Mössbauer spectra of staurolite and reached "no firm conclusion regarding the presence of octahedral Fe^{2+}." In a study of the temperature dependence of the Mössbauer spectra of 15 staurolites, Dzhemats and Nikitina (1977) fit the spectra with up to five doublets and concluded that the Fe is distributed among octahedral sites as well as energetically nonequivalent tetrahedral sites. In yet another temperature-dependence study, Varma and Varma (1986) resolved their spectra into four doublets, two of which they attributed to divalent Fe in tetrahedral sites and the other two to trivalent Fe in octahedral sites.

In addition to Mössbauer spectroscopy, other methods have been used in attempts to solve the Fe-distribution problem in staurolite. Griffen and Ribbe (1973) applied principal-component analysis to two sets of chemical analyses of staurolites. They concluded that Fe exists in both octahedral and tetrahedral coordination and that Al and Zn are more important than Mg as substituents at the **Fe** site. This conclusion was later supported by Ward (1984a), who examined the relationships between unit-cell parameters and Mg contents in some high-Mg staurolites. A different Fe-distribution scheme was proposed by Tagai and Joswig (1985) who refined the crystal structure from neutron-diffraction data. A small amount (8%) of the Fe was assigned to the **Si** site, on the basis of the neutron-scattering lengths of the cations in the site, and the remaining Fe was assigned to the **Fe** and **U** sites on the basis of the interatomic distances in the **Al(3)** octahedra. Holdaway et al. (1986b) also addressed the Fe-distribution problem. From their chemical analyses of 31 staurolites and Smith's (1968) structure refinement, they concluded that the kyanite-layer sites are occupied mainly by Si and Al, the **Al(3)** sites by Al and Fe^{3+}, the **U** sites by Mn and Fe^{2+}, and the **Fe** site by Fe^{2+}, Mg, Ti, Li, and Zn. Their results differed from those of Griffen and Ribbe (1973) in that they found Mg to be more important than Al as a substituent in the **Fe** site. They attributed the difference to the lack of accurate H^+ analyses in the Griffen and Ribbe (1973) study.

The present study addresses the Fe-distribution problem by focusing on two related issues: (1) the distribution of Fe among various possible sites and (2) the significance of apparent positional and/or temporal disorder at the **Fe** site. A sample of staurolite from Franklin County, North Carolina (USNM 106038), was obtained from D. T. Griffen. Crystal-structure refinements at room and nominal liquid-N_2 temperatures were compared with Mössbauer spectra, also obtained at room and liquid-N_2 temperatures, in order to determine the distribution of Fe in this particular staurolite.

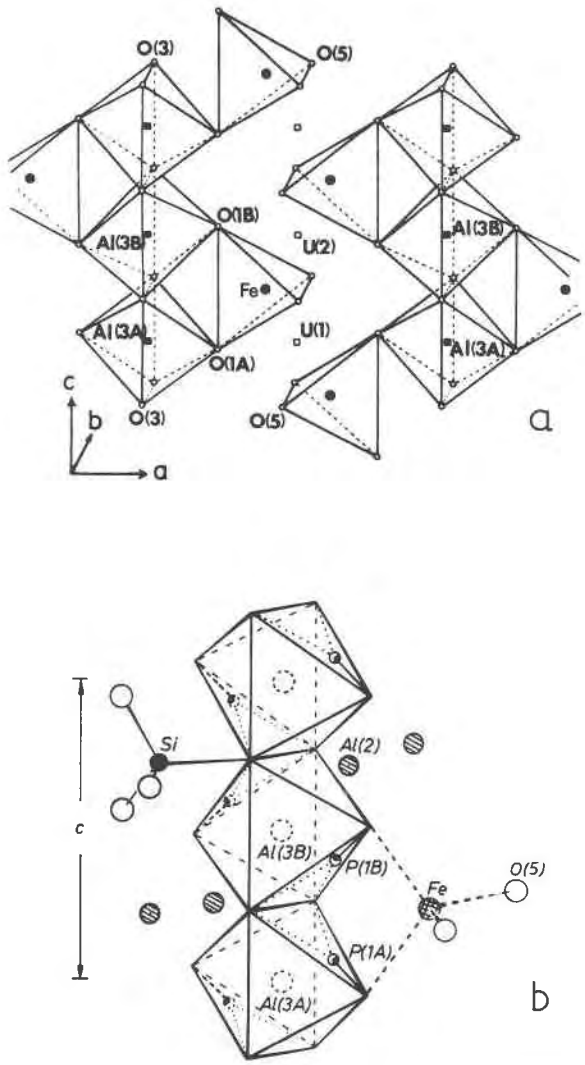

Fig. 1. The crystal structure of the monolayer in staurolite, (**a**) showing cation and oxygen sites and (**b**) showing locations of the H sites [**P(1A)** and **P(1B)**]. After Holdaway et al. (1986b).

Procedures and results

Crystal structure

Data collection. The crystal selected for collection of X-ray–diffraction data was roughly tetrahedral in shape, 0.4 mm on a side. A Nicolet P3 automated four-circle single-crystal diffractometer was used with Mo$K\alpha$ X-radiation. During low-temperature data collection, N_2 gas, cooled by passing through liquid N_2, was constantly blown over the crystal. The actual temperature attained by the cryogenic device is estimated to be 123 K. The same set of reflections was collected under identical machine settings at both room and low temperatures, with the exception of about 50 reflections that were outside the physical range of the low-temperature device. Based on space group $C2/m$, a set of unique reflections and their Friedel counterparts were collected. R factors for equivalent reflec-

Table 1. Lattice parameters

Parameter	Room temperature	Low temperature
a (Å)	7.865(2)	7.871(2)
b (Å)	16.580(4)	16.587(5)
c (Å)	5.668(3)	5.661(3)
β (°)	90.38(5)	90.39(7)
V (Å^3)	739.1(3)	739.1(4)

Note: Numbers in parentheses are esd's.

tions, which were automatically averaged during the data reduction, were 0.009 for the room-temperature data and 0.010 for the low-temperature data. A θ–2θ scan mode was used with an upper 2θ limit of 60°. The scan rate and width were varied depending on diffraction intensity and Bragg angle, respectively. Three check reflections, collected once in every 100 reflections, showed variations in intensity of less than 6%, and the crystal was automatically recentered every 1000 reflections. Background and Lorentz-polarization corrections were made following data collection.

Lattice parameters shown in Table 1 were determined by least-squares refinement of the 25 reflections used to center the crystal for data collection. The same reflections were used in calculating lattice parameters at both room and low temperatures.

Crystal-structure refinement. The crystal structure was refined using the program SHELX-76 (Sheldrick, 1976). Starting parameters were taken from Smith (1968), scattering-factor coefficients from Cromer and Mann (1968), and anomalous scattering factors and mass-absorption coefficients from Cromer and Liberman (1970). The refinement was begun with the room-temperature data and neutral-atom scattering factors for Fe, Si, Al, and O. Only positional parameters were allowed to vary during the first few cycles, then isotropic temperature factors were refined. Next, anisotropic temperature factors were introduced for all sites except the low-occupancy **U(1)** and **U(2)** sites. The temperature factors were allowed to vary alternately with the cation-site occupancies for a few cycles before all parameters were refined together.

The refinement of the low-temperature data proved to be more sensitive to the site-occupancy model represented by the scattering factors. Since the scattering power of a site depends on the type of atom in the site, the scattering power of a site containing several different species can be approximated by the scattering factor of an "average" atom determined by $A = (\Sigma\ a_i n_i)/N$, where A is the atomic number of the average atom, a_i the atomic number of each species, n_i the number of atoms of each species at the site, and N the total number of atoms in the site. Various scattering factors representing different cation-site occupancy models were tried in the structure refinement. The final site occupancy model is listed in Table 2. Problems were encountered when the scattering factors necessary to avoid nonpositive-definite temperature factors for some sites required heavier model atoms than the chemical formula, determined by microprobe analysis, provided. Use of ionic scattering factors for all sites eliminated the problem. Once an acceptable site-occupancy model was established, absorption corrections were made on both data sets using appropriate scattering factors and the method of Walker and Stuart (1983).

A difference-Fourier map (Fig. 2) showed three distinct peaks around the **Fe** site similar to those noted by Smith (1968) and Bringhurst and Griffen (1986). The peak positions on this map are nearly the same as Smith's (1968), but the relative peak heights more closely resemble those of Bringhurst and Griffen (1986) in that **Fe1** (Smith's C) is the largest and **Fe3** (Smith's B) is the smallest. The positions of these peaks were used as starting parameters for dividing the **Fe** site into three subsites, resulting in a decrease of 0.002 in the conventional residuals. Occupancies for the **Fe** subsites are listed in Table 3. Although disorder at the **Fe** site appears to be an intrinsic feature of staurolite, a model with three **Fe** subsites does not represent a significant improvement over the model with one **Fe** site for two reasons: First, the precision of the structure refinement is questionable for such closely spaced sites, as evidenced by correlation coefficients of 0.9 or greater between some positional parameters and the **Fe**-subsite occupancies. Second, the number of **Fe** subsites

Table 2. Cation-site occupancies

Cation site	Postulated occupancy (in numbers of atoms)	Model-atom occupancy*	Observed occupancy**		Fractional occupancy†
			Room temp.	Low temp.	
Fe	0.07 Al, 0.09 Ti, 0.65 Zn, 0.93 Mg, 2.14 Fe^{2+}	0.97 (V^{2+})	0.966(4)	0.976(4)	0.97
Si	7.22 Si, 0.78 Al	0.99 (Si^{4+})	0.995(4)	1.002(4)	1.00
Al(1A)	3.79 Al	0.95 (Al^{3+})	0.942(5)	0.945(5)	0.95
Al(1B)	3.84 Al	0.96 (Al^{3+})	0.957(5)	0.961(6)	0.96
Al(2)	7.79 Al	0.97 (Al^{3+})	0.964(5)	0.971(5)	0.97
Al(3A)	1.145 Al, 0.095 Fe^{3+}	0.62 (Si^{4+})	0.614(7)	0.622(7)	0.62
Al(3B)	0.595 Al, 0.045 Fe^{3+}	0.32 (Si^{4+})	0.318(6)	0.318(6)	0.32
U(1)	0.05 Mn, 0.03 Fe^{2+}	0.04 (Mn^{2+})	0.042(3)	0.043(3)	0.04
U(2)	0.03 Mn, 0.01 Fe^{2+}	0.02 (Mn^{2+})	0.022(3)	0.024(3)	0.02

* Occupancy based on scattering power of model atom (listed in parentheses).
** Site occupancy from crystal-structure refinements.
† Number of atoms (of any species) divided by number of sites.

TABLE 3. Occupancies of the **Fe** subsites

Subsite	Observed occupancy*		Percent of total Fe-site cations	
	RT	LT	RT	LT
Fe1	0.45(8)	0.48(9)	0.46	0.49
Fe2	0.17(4)	0.17(5)	0.18	0.18
Fe3	0.35(8)	0.32(8)	0.36	0.33

* Site occupancy from crystal-structure refinement at room temperature (RT) and low temperature (LT).

has not been well established. A difference-Fourier map through the **Fe** site of the refinement for three **Fe** subsites showed some anomalous electron density (possibly due to the necessity of using isotropic temperature factors for the **Fe** subsites) that may indicate the presence of other (minor) occupied positions in the **Fe** tetrahedron in addition to the three previously observed subsites. For these reasons, all data presented in this paper will be from the model with one **Fe** site unless otherwise noted.

Both room- and low-temperature refinements were completed using absorption-corrected data and anisotropic temperature factors for all sites except the low-occupancy **U** sites and the strongly overlapping **Fe** subsites. Final conventional residuals for the room-temperature refinements, with three **Fe** subsites and one **Fe** site were 0.029 and 0.031, respectively, for the 1093 reflections with $I > 3\sigma(I)$; for the low-temperature refinements, they were 0.030 and 0.032, respectively, for 1097 reflections with $I > 3\sigma(I)$. Observed and calculated structure factors are listed in Table 4.[1] Table 5 contains the final positional parameters and temperature-factor coefficients. Bond lengths and angles are listed in Table 6.

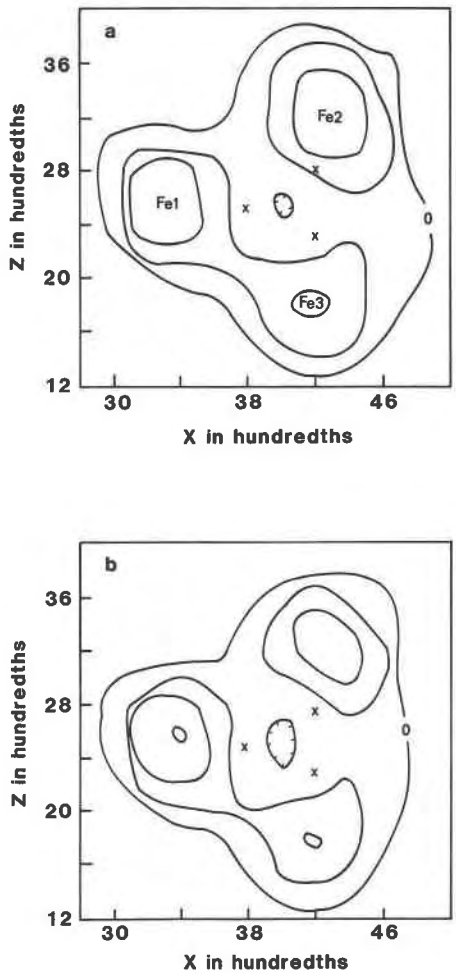

Fig. 2. (**a**) Room-temperature and (**b**) low-temperature electron-density difference maps of staurolite (USNM 106038) at $y = 0$ in the vicinity of the **Fe** site. Refined positions of the **Fe** subsites are indicated by x's. Contour interval is approximately 0.3 electrons per cubic angstrom.

Optical properties

The crystal used for X-ray data collection was mounted on a spindle stage for determination of optical properties. Indices of refraction, measured in Na_D light with standard oil-immersion techniques, are $\alpha = 1.738$, $\beta = 1.743$, and $\gamma = 1.747$ (all ± 0.002). The computer program EXCALIBR (Bloss, 1981) was used to determine the $2V_X$ angle of 89.5(7)° from extinction-curve data, in reasonable agreement with the $2V_X$ angle calculated from the indices of refraction (83.6°).

This staurolite is optically negative and contains relatively high concentrations of Zn (Table 7). Griffen (1981) also found a synthetic Zn end-member staurolite to be optically negative. Bringhurst and Griffen (1986) noted the same property in their cobaltoan staurolite and attributed it to low numbers of transition-metal atoms rather than to the presence of Co. The ionic refractivity of Zn is about two-thirds that of Fe (Batsanov, 1959, p. 60), so 2.33 Fe atoms combined with 0.65 Zn atom would be optically equivalent to about 2.7 Fe atoms, which yields a $2V_X$ of about 87° from Figure 1 of Griffen and Ribbe (1973), in good agreement with the measured $2V_X$ of 89.5°.

Microprobe analysis

The crystal was mounted in epoxy and analyzed using the ARL microprobe at the University of Utah. Standards used were anorthite for Si and Al, olivine for Mg and Fe, pyroxene for Mn, titanium oxide for Ti, chromite for Cr, vanadinite for V, synthetic sphalerite for Zn, and Co metal for Co. The raw data were reduced to oxide weight percentages using ZAF corrections.

Chemical formulas were calculated according to two different estimates of the H^+ content, one from an earlier chemical analysis of this staurolite and the other based

[1] A copy of Table 4 may be ordered as Document AM-89-405 from the Business Office, Mineralogical Society of America, 1625 I Street, N.W., Suite 414, Washington, D.C. 20006, U.S.A. Please remit $5.00 in advance for the microfiche.

TABLE 5. Final atomic positional parameters and temperature factor coefficients ($\times 10^4$)

Site	x	y	z	U_{11}*	U_{22}*	U_{33}*	U_{23}*	U_{13}*	U_{12}*
				Room temperature					
Fe	0.3897(1)	0.0	0.2471(1)	150(3)	65(3)	164(3)	0	−3(2)	0
Fe1**	0.3778(20)	0.0	0.2497(16)	73(10)					
Fe2**	0.4027(22)	0.0	0.2783(43)	39(23)					
Fe3**	0.3994(20)	0.0	0.2291(31)	67(14)					
Si	0.1342(1)	0.1662(0)	0.2482(1)	40(3)	63(3)	40(3)	−1(2)	0(2)	0(2)
Al(1A)	0.5	0.1751(1)	0.0	29(4)	48(5)	9(4)	0	−2(3)	0
Al(1B)	0.5	0.1749(1)	0.5	38(4)	58(5)	18(4)	0	6(3)	0
Al(2)	0.2628(1)	0.4104(0)	0.2518(1)	39(3)	60(3)	52(3)	1(3)	−1(2)	−2(2)
Al(3A)	0.0	0.0	0.0	78(10)	86(10)	88(11)	0	26(7)	0
Al(3B)	0.0	0.0	0.5	52(18)	65(18)	81(20)	0	−31(13)	0
U(1)	0.5	0.0	0.0	19(40)					
U(2)	0.5	0.0	0.5	175(107)					
O(1A)	0.2328(3)	0.0	0.9628(4)	126(11)	80(10)	75(11)	0	16(8)	0
O(1B)	0.2358(3)	0.0	0.5339(4)	153(11)	89(11)	83(11)	0	2(9)	0
O(2A)	0.2558(2)	0.1614(1)	0.0152(3)	71(7)	87(7)	61(7)	−5(6)	−2(5)	3(5)
O(2B)	0.2545(2)	0.1610(1)	0.4835(3)	79(7)	88(7)	56(7)	9(5)	4(5)	−3(5)
O(3)	0.0015(2)	0.0889(1)	0.2447(3)	63(7)	100(7)	119(7)	−4(6)	0(6)	3(6)
O(4)	0.0218(2)	0.2493(1)	0.2493(3)	72(7)	83(7)	59(7)	3(6)	−1(5)	7(6)
O(5)	0.5270(2)	0.0996(1)	0.2495(3)	49(7)	90(7)	46(7)	0(6)	−1(5)	−11(5)
				Low temperature					
Fe	0.3901(1)	0.0	0.2472(1)	129(3)	48(3)	137(3)	0	−3(2)	0
Fe1**	0.3789(20)	0.0	0.2496(16)	57(9)					
Fe2**	0.4031(25)	0.0	0.2765(47)	26(24)					
Fe3**	0.4001(22)	0.0	0.2290(35)	44(16)					
Si	0.1342(1)	0.1662(0)	0.2482(1)	31(3)	56(3)	31(3)	0(2)	0(2)	−1(2)
Al(1A)	0.5	0.1751(1)	0.0	17(4)	35(5)	3(5)	0	0(3)	0
Al(1B)	0.5	0.1749(1)	0.5	28(4)	44(5)	11(5)	0	3(3)	0
Al(2)	0.2627(1)	0.4104(0)	0.2518(1)	27(3)	48(3)	37(4)	1(3)	0(2)	0(2)
Al(3A)	0.0	0.0	0.0	79(10)	67(10)	79(11)	0	23(7)	0
Al(3B)	0.0	0.0	0.5	43(18)	46(18)	67(21)	0	−21(14)	0
U(1)	0.5	0.0	0.0	10(40)					
U(2)	0.5	0.0	0.5	176(100)					
O(1A)	0.2332(3)	0.0	0.9628(4)	107(11)	69(10)	57(11)	0	17(9)	0
O(1B)	0.2361(3)	0.0	0.5339(4)	130(11)	78(11)	64(12)	0	2(9)	0
O(2A)	0.2559(2)	0.1614(1)	0.0150(3)	51(7)	74(7)	53(7)	0(6)	−3(6)	5(5)
O(2B)	0.2547(2)	0.1609(1)	0.4837(3)	60(7)	68(7)	48(7)	4(6)	5(6)	−2(5)
O(3)	0.0016(2)	0.0889(1)	0.2446(3)	57(7)	87(7)	97(8)	0(6)	−4(6)	4(6)
O(4)	0.0217(2)	0.2492(1)	0.2492(3)	56(7)	69(7)	50(7)	2(6)	−2(6)	5(6)
O(5)	0.5270(2)	0.0996(1)	0.2496(3)	40(7)	80(7)	33(7)	−3(6)	−4(5)	−14(5)

* U_{ij} are coefficients in the expression $\exp[-2\pi^2(a^{*2}U_{11}h^2 + b^{*2}U_{22}k^2 + c^{*2}U_{33}l^2 + 2a^*b^*U_{12}hk + 2a^*c^*U_{13}hl + 2b^*c^*U_{23}kl)]$.
** **Fe**-subsite parameters are taken from the refinement with three **Fe** sites. All others come from the refinement with one **Fe** site.

on the observed site occupancies of the present structure refinement. Previous chemical analyses of this staurolite found 3.023 H^+ and 0.011 Li^+ ions (Dutrow et al., 1986; Holdaway et al., 1986a, 1986b). Table 7 lists the oxide weight percentages, the chemical formula resulting when these amounts of H^+ and Li^+ are assumed, and the chemical formula resulting when the maximum H^+ content (according to the present refinement) is assumed. The maximum H^+ content was estimated following the reasoning of Takéuchi et al. (1972) that a proton site can only be occupied when its adjacent **Al(3)** site is not. The fractional occupancies of the **Al(3A)** and **Al(3B)** sites are 0.62 and 0.32, respectively. This leaves 2.12 vacancies in the **Al(3)** octahedra or a maximum of 4.24 occupied proton sites per 48-oxygen formula unit. Holdaway et al. (1986b) have suggested more accurate methods for estimating the H^+ and Li^+ contents of staurolite based on associations with other minerals. However, complete mineral associations for this staurolite are unknown, so these methods could not be applied.

The chemical formulas were first calculated with the assumption that all Fe is Fe^{2+}. Later, when the crystal-structure refinements were complete and the Mössbauer spectra were obtained, the suggestion of Holdaway et al. (1986b)—that all Fe in the **Al(3)** sites is Fe^{3+}—was followed. The chemical formulas were recalculated on the basis of 6% of the Fe being Fe^{3+}, the amount of Fe assigned to the **Al(3)** sites in the site-occupancy model for the crystal-structure refinement. This is supported by Mössbauer data, presented below, which indicate that 5–10% of the Fe is Fe^{3+}.

The number of cations in the chemical formula with all Fe as Fe^{2+} turned out to be about 0.9% more than the site occupancies (determined during the structure refinement) could accommodate. This number changed to 0.7% when 6% of the Fe was assumed to be Fe^{3+}. In order to distribute the discrepancy evenly among the cation species before making final cation-site assignments, a correction factor was determined that was based on the relative scattering powers of the ions in the chemical formulas and

TABLE 6. Interatomic distances and angles

Atoms	Distances (Å) RT	Distances (Å) LT	Atoms	Distances (Å) RT	Distances (Å) LT	Angles (°) RT	Angles (°) LT
			Fe tetrahedron				
Fe–O(1A)	2.023(2)	2.022(2)	O(1A)–O(1B)	3.237(3)	3.233(3)	105.9	105.8
–O(1B)	2.033(2)	2.032(3)	–O(5)	3.267(3) ×2	3.265(3) ×2	109.7 ×2	109.6 ×2
–O(5)	1.973(2) ×2	1.972(2) ×2	O(1B)–O(5)	3.259(3) ×2	3.258(3) ×2	108.9 ×2	108.9 ×2
Mean	2.001	2.000	O(5)–O(5)	3.303(3)	3.304(3)	113.6	113.8
			Mean	3.265	3.264		
			Si tetrahedron				
Si–O(2A)	1.638(2)	1.638(2)	O(2A)–O(2B)	2.654(2)	2.653(2)	108.5	108.4
–O(2B)	1.632(2)	1.633(2)	–O(3)	2.678(2)	2.679(2)	109.0	109.0
–O(3)	1.653(2)	1.653(2)	–O(4)	2.703(2)	2.704(2)	111.2	111.3
–O(4)	1.637(2)	1.637(2)	O(2B)–O(3)	2.680(2)	2.682(2)	109.4	109.4
Mean	1.640	1.640	–O(4)	2.688(2)	2.690(2)	110.6	110.7
			O(3)–O(4)	2.664(2)	2.664(2)	108.2	108.1
			Mean	2.678	2.679		
			Al(1A) octahedron				
Al(1A)–O(2A)	1.937(2) ×2	1.937(2) ×2	O(2A)–O(4)	2.880(2) ×2	2.880(2) ×2	97.4 ×2	97.4 ×2
–O(4)	1.896(2) ×2	1.895(2) ×2	–O(4)	2.745(2) ×2	2.745(2) ×2	91.5 ×2	91.5 ×2
–O(5)	1.900(2) ×2	1.899(2) ×2	–O(5)	2.707(2) ×2	2.707(2) ×2	89.8 ×2	89.8 ×2
Mean	1.911	1.910	–O(5)	2.501(2) ×2	2.500(2) ×2	81.4 ×2	81.3 ×2
			O(4)–O(4)	2.845(3)	2.840(3)	97.2	97.0
			–O(5)	2.506(2) ×2	2.508(2) ×2	82.6 ×2	82.8 ×2
			O(5)–O(5)	2.857(3)	2.855(3)	97.6	97.5
			Mean	2.698	2.698		
			Al(1B) octahedron				
Al(1B)–O(2B)	1.946(2) ×2	1.946(2) ×2	O(2B)–O(4)	2.904(2) ×2	2.905(2) ×2	97.8 ×2	97.9 ×2
–O(4)	1.906(2) ×2	1.906(2) ×2	–O(4)	2.751(2) ×2	2.752(2) ×2	91.1 ×2	91.2 ×2
–O(5)	1.904(2) ×2	1.902(2) ×2	–O(5)	2.725(2) ×2	2.724(2) ×2	90.1 ×2	90.1 ×2
Mean	1.919	1.918	–O(5)	2.499(2) ×2	2.496(2) ×2	81.0 ×2	80.9 ×2
			O(4)–O(4)	2.865(3)	2.862(3)	97.5	97.3
			–O(5)	2.506(2) ×2	2.508(2) ×2	82.3 ×2	82.4 ×2
			O(5)–O(5)	2.874(3)	2.870(3)	98.0	97.9
			Mean	2.709	2.709		
			Al(2) octahedron				
Al(2)–O(1A)	1.921(2)	1.920(2)	O(1A)–O(1B)	2.431(3)	2.428(3)	78.6	78.5
–O(1B)	1.919(2)	1.918(2)	–O(2A)	2.698(2)	2.699(2)	89.0	89.1
–O(2A)	1.930(2)	1.928(2)	–O(3)	2.631(2)	2.634(3)	87.7	87.7
–O(2B)	1.917(2)	1.914(2)	–O(5)	2.788(2)	2.787(2)	95.0	94.9
–O(3)	1.878(2)	1.881(2)	O(1B)–O(2B)	2.689(2)	2.688(2)	89.0	89.1
–O(5)	1.862(2)	1.863(2)	–O(3)	2.695(2)	2.698(3)	90.4	90.5
Mean	1.905	1.904	–O(5)	2.772(2)	2.771(2)	94.3	94.2
			O(2A)–O(2B)	3.014(2)	3.008(2)	103.1	103.1
			–O(3)	2.770(2)	2.770(2)	93.3	93.3
			–O(5)	2.501(2)	2.500(2)	82.5	82.5
			O(2B)–O(3)	2.810(2)	2.811(2)	95.6	95.6
			–O(5)	2.499(2)	2.496(2)	82.8	82.7
			Mean	2.692	2.691		
			Al(3A) octahedron				
Al(3A)–O(1A)	1.845(2) ×2	1.849(2) ×2	O(1A)–O(3)	2.841(2) ×4	2.843(3) ×4	94.4 ×4	94.4 ×4
–O(3)	2.024(2) ×4	2.023(2) ×4	–O(3)	2.631(2) ×4	2.634(3) ×4	85.6 ×4	85.6 ×4
Mean	1.964	1.965	O(3)–O(3)	2.948(3) ×2	2.949(3) ×2	93.5 ×2	93.6 ×2
			–O(3)	2.774(3) ×2	2.769(3) ×2	86.5 ×2	86.4 ×2
			Mean	2.778	2.779		
			Al(3B) octahedron				
Al(3B)–O(1B)	1.863(2) ×2	1.867(2) ×2	O(1B)–O(3)	2.866(2) ×4	2.867(3) ×4	93.6 ×4	93.5 ×4
–O(3)	2.066(2) ×4	2.065(2) ×4	–O(3)	2.695(2) ×4	2.698(3) ×4	86.5 ×4	86.5 ×4
Mean	1.998	1.999	O(3)–O(3)	2.948(3) ×2	2.949(3) ×2	91.1 ×2	91.1 ×2
			–O(3)	2.894(3) ×2	2.892(3) ×2	89.0 ×2	88.9 ×2
			Mean	2.827	2.829		
			U(1) octahedron				
U(1)–O(1A)	2.111(2) ×2	2.109(2) ×2	O(1A)–O(5)	3.267(2) ×4	3.265(2) ×4	99.0 ×4	99.0 ×4
–O(5)	2.184(2) ×4	2.183(2) ×4	–O(5)	2.788(2) ×4	2.787(2) ×4	81.0 ×4	81.0 ×4
Mean	2.160	2.158	O(5)–O(5)	3.303(3) ×2	3.304(3) ×2	98.3 ×2	98.3 ×2
			–O(5)	2.857(3) ×2	2.855(3) ×2	81.7 ×2	81.7 ×2
			Mean	3.045	3.044		
			U(2) octahedron				
U(2)–O(1B)	2.088(2) ×2	2.087(2) ×2	O(1B)–O(5)	3.259(2) ×4	3.258(2) ×4	99.2 ×4	99.3 ×4
–O(5)	2.189(2) ×4	2.188(2) ×4	–O(5)	2.772(2) ×4	2.771(2) ×4	80.8 ×4	80.8 ×4
Mean	2.155	2.154	O(5)–O(5)	3.303(3) ×2	3.304(3) ×2	97.9 ×2	98.1 ×2
			–O(5)	2.874(3) ×2	2.870(3) ×2	82.1 ×2	82.0 ×2
			Mean	3.040	3.039		

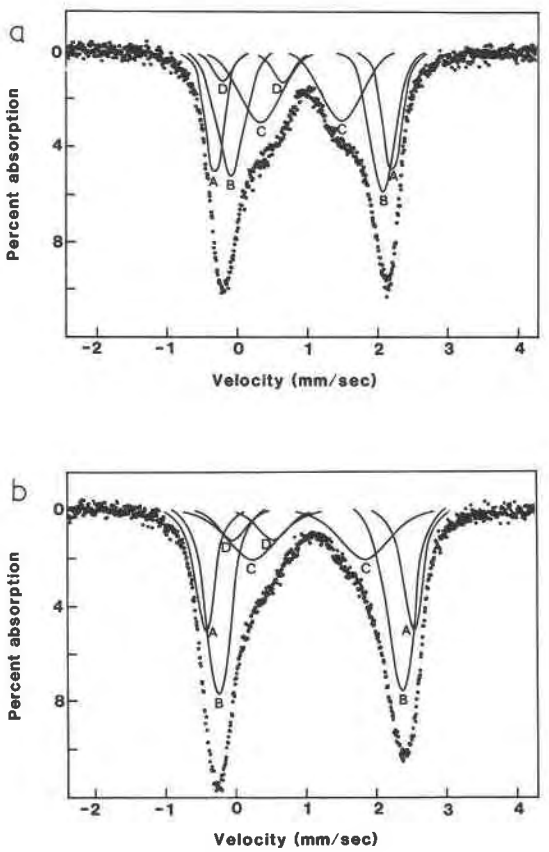

Fig. 3. Mössbauer spectra of staurolite (USNM 106038) at (**a**) room temperature and (**b**) liquid-N_2 temperature. Metallic Fe is the reference material.

the refined site occupancies. Scattering powers were determined by the following equations:

$$S_{\text{structure refinement}} = \Sigma\, K_i A_i,$$

where S is the scattering power, K_i is the occupancy of each site, and A_i is the atomic number of the average atom for that site, and

$$S_{\text{chemical formula}} = \Sigma\, n_i a_i,$$

Table 7. Microprobe analysis

Oxide*	wt%	Cations for H(max) = 4.2	Cations for Li = 0.011 H = 3.023**
MgO	2.32	0.94	0.95
Al_2O_3	56.59	18.10	18.33
SiO_2	26.74	7.26	7.35
TiO_2	0.42	0.09	0.09
MnO	0.34	0.08	0.08
FeO	9.66	2.19	2.22
Fe_2O_3	0.69	0.14	0.14
ZnO	3.24	0.65	0.66
Total	100.00		

* V, Cr, and Co were not found in detectable amounts.
** Li and H values from Holdaway et al. (1986b).

Table 8. Mössbauer parameters and peak areas

	CS (mm/s)		QS (mm/s)		Γ (mm/s)		*A* (%)	
Doublet	RT	LT	RT	LT	RT	LT	RT	LT
A (Fe^{2+})	0.96	1.07	2.50	2.93	0.29	0.30	23.3	20.7
B (Fe^{2+})	0.98	1.04	2.13	2.52	0.46	0.44	39.5	46.0
C (Fe^{2+})	0.92	1.00	1.17	1.60	0.66	0.83	30.8	23.9
D (Fe^{3+})	0.60	0.27	0.83	0.58	0.29	0.52	6.4	9.4

Note: CS is the center shift, QS is the quadrupole splitting, Γ is the line width, and *A* is the relative area inside each doublet.

where n_i is the number of atoms of each type and a_i is the atomic number of each type of atom. Since the scattering power of the "maximum H^+" formula (with 6% Fe^{3+}) was closest to that determined by the structure refinement, this chemical formula was multiplied by a factor of 0.995 from the ratio

$$S_{\text{structure refinement}}/S_{\text{chemical formula}}.$$

All references to the chemical composition of this staurolite are made based on the corrected maximum H^+ chemical formula.

Mössbauer spectroscopy

Mössbauer spectra at room and liquid N_2 temperatures (293 K and 77 K, respectively) were obtained from a powdered portion of the staurolite sample (Fig. 3). The spectra are fit to three Fe^{2+} doublets and one Fe^{3+} doublet with $\chi^2 = 1.2$ and 1.3 for the room- and low-temperature spectra, respectively. Fits with only two Fe^{2+} doublets resulted in χ^2 values of 2.1 and 4.6 for the two spectra, respectively. Mössbauer parameters and relative peak areas are listed in Table 8. The dips and widths of the components of doublets A, C, and D were constrained to be equal. Doublet B was left unconstrained as a test of the validity of an eight-peak fit. The high- and low-velocity peaks of doublet B showed only slight differences in area (2% at room temperature and 4% at low temperature), indicating that the number of peaks fit to the spectra is not unreasonable. Estimated minimum errors for the Mössbauer parameters were calculated using the method of Dollase (1975) and are listed in Tables 9 and 10. Three limitations on the interpretation of these Mössbauer spectra should be noted. First, doublet D (Fe^{3+}) is not very well defined, as is indicated by the unreasonably large changes in line width, center shift, and quadrupole splitting with temperature (Table 8). The estimated errors in peak areas for this doublet are also very large (Table 10). Although a small amount of Fe^{3+} (~5–10% of the Fe) does seem to be present in this staurolite, nothing more can be derived from Mössbauer data concerning Fe^{3+} in this specimen. Second, changes in the relative areas of the Fe^{2+} peaks with temperature are within the estimated errors of the peak areas (Table 10), and therefore the apparent temperature dependence of the relative areas of these peaks may be an artifact of the curve fitting. Third, the large line widths and the increase in line widths with temper-

TABLE 9. Estimated errors for Mössbauer parameters

Doublet	ϵ_x (%)		ϵ_w (%)	
	RT	LT	RT	LT
A	0.5	0.4	1.6	1.5
B (avg)	0.4	0.2	1.1	0.6
C	0.5	0.6	1.6	1.7
D	1.9	1.4	5.0	4.0

Note: ϵ_x (error in peak position) and ϵ_w (error in peak width) are functions of peak dip, width, and background counts and are based on the assumption that all peaks are isolated. The dips and widths of the high- and low-velocity peaks of doublets A, C, and D were constrained to be equal.

TABLE 10. Estimated errors in Mössbauer peak areas due to overlap of peaks

Doublet	ϵ_a (%) due to overlap with doublet					
	A		B		C	
	RT	LT	RT	LT	RT	LT
A	—	—	13	8	2	2
B	9	4	—	—	2	3
C	2	3	4	8	—	—
D	5	4	5	4	29	36

Note: Errors in peak areas (ϵ_a) depend on peak separation (calculated using an average of the two line widths), and peak size relative to background. ϵ_a values are listed for high-velocity peaks only. Errors for doublet D are due to overlap with the low-velocity peaks of doublets A, B, and C; all other errors result from overlap with high-velocity peaks.

ature of doublet C indicate that this doublet is probably composed of two or more closely overlapping smaller doublets.

DISCUSSION

Cation-site assignments

Table 2 lists the estimated occupancies of the cation sites in this staurolite. In agreement with most previous workers (Smith, 1968; Ward, 1984a; Bringhurst and Griffen, 1986; Holdaway et al., 1986b), all available Si plus enough Al to fill the site were assigned to the **Si** site. However, some evidence exists in support of Tagai and Joswig (1985), who assigned a small amount of Fe to the **Si** site. The observed occupancy of the **Si** site in the present staurolite is 100%. Since only 7.22 atoms of Si are available, filling the remaining site vacancies with Al to the observed occupancy would give a fractional occupancy of 101%. Adding a small amount of Fe to the postulated occupancy of the **Si** site would lower the fractional occupancy while keeping the model-atom occupancy equal to the observed occupancy. Any Fe in the **Si** site would be Fe^{3+}, a small amount of which is probably present in this staurolite, as mentioned previously. Also, as in previous models, Mn was assigned to the **U** sites (Smith, 1968), and Zn and Ti to the **Fe** site (Griffen, 1981; Ward, 1984b). For simplicity, all Mg was assigned to the **Fe** site, and Al was assumed to be the sole occupant of the **Al(1A)**, **Al(1B)**, and **Al(2)** sites, following Holdaway et al. (1986b). However, since Mg and Al are indistinguishable by X-ray diffraction methods, Mg could also have been assigned to the various **Al** sites, thus requiring more Al in the **Fe** site. A small amount of Al was needed in the **Fe** site to fill it to its observed occupancy, and the remainder was assigned to the **Al(3)** sites along with enough Fe to raise the average atomic numbers of the sites to 14, the lowest model-atom scattering factor that did not cause non–positive-definite temperature factors for these sites in the structure refinement. The Fe assigned to the **Al(3)** sites was assumed to be Fe^{3+}, following Holdaway et al. (1986b), and the chemical formula was recalculated with this amount of Fe (6%) as Fe^{3+}. The recalculated chemical formula required no changes in the final cation-site assignments, so the model would remain the same if all Fe was assumed to be Fe^{2+}.

Distribution of Fe

Mössbauer spectra of this staurolite were obtained at room and liquid-N_2 temperatures in order to build a model of Fe distribution for the structure refinement. Exactly the opposite occurred, however, since the structure refinement, through the scattering power at each site, provided enough of its own limits on the locations of the Fe. Other workers (Smith, 1968; Takéuchi et al., 1972; Bringhurst and Griffen, 1986) who have compared crystal-structure refinements with Mössbauer spectra of staurolite have resolved the spectra into two doublets, one representing tetrahedrally coordinated Fe^{2+} (~75%) and the other representing octahedrally coordinated Fe^{2+} (~25%). When this model was used with the present structure refinement, the model atom for the **Fe** site could not be made heavy enough to match the calculated occupancy of the site without filling it to 107% fractional occupancy. On the other hand, following Dowty's (1972) interpretation by assuming all the Fe to be tetrahedrally coordinated resulted in non–positive-definite temperature factors for the **Al(3)** sites. [Following the suggestion of Schreyer et al. (1984)—i.e., assigning all available Ti to the **Al(3)** sites—provides only half the scattering power needed to change the model atom for these sites from atomic number 13 to number 14.] On the basis of the structure refinement alone, the following distribution of Fe is derived: 92% in $^{[4]}$**Fe**, 6% in $^{[6]}$**Al(3)**, and 2% in $^{[6]}$**U**. This model could vary, of course, depending on the actual distribution of Mg in the crystal structure. A small amount of Mg at the **Al(3)** sites would require more Fe to compensate for Mg's lower atomic number compared to Al. The variation would be slight, however, and the Fe distribution would remain essentially the same.

Ordering considerations at the Fe site

At first glance, the Mössbauer spectra appear to conflict with the results of the structure refinement. Most (92%) of the Fe is located at the **Fe** site, yet the Mössbauer spectra clearly show more than one set of peaks, with about 50% of the Fe distributed among the smaller peaks. Mössbauer spectral parameters depend on the valence states, coor-

dination numbers, and crystal-field splittings at the Fe sites (Hawthorne, 1983). Most, if not all, the Fe in the present staurolite is Fe^{2+}, as previously noted, so valence states will not have much effect on the Mössbauer parameters. Coordination numbers have been established through the crystal-structure refinement and indicate that all three Fe^{2+} Mössbauer doublets arise from the $^{[4]}$**Fe** site. This leaves crystal-field variations to explain the number of Mössbauer doublets that are present. If each Mössbauer doublet arises from Fe in a different crystal-field environment, then there must be three major types of **Fe** sites and possibly several minor types of **Fe** sites, as well as minor octahedral Fe sites, as indicated by the large line widths of doublet C.

The positional disorder indicated by the electron-density difference map (Fig. 2) from the structure refinement also suggests that there are at least three types of **Fe** sites. Bringhurst and Griffen (1986) summarized three possible explanations for positional disorder at the **Fe** site in staurolite: (1) cation-cation repulsion between the **Fe** and **U** sites, (2) metal-metal bonding attraction between the **Fe** and **U** sites, and (3) proton-cation repulsion between the **P** and **Fe** sites (Fig. 1). The major shortcoming of the first two proposals is the low occupancy of the **U** sites. The **Fe** site could only be affected if one or both neighboring **U** sites were occupied, which is true for, at most, 6% of the **Fe** sites (Table 2). The most highly occupied **Fe** subsite (**Fe1**) contains about 50% of the cations in the **Fe** site (Table 3), implying that at least half of the cations in the **Fe** site are being influenced by whatever mechanism is causing the positional disorder at the **Fe** site.

The proton-cation repulsion explanation [also proposed by Holdaway et al. (1986b)] implies control of the **Fe** subsite occupancies by occupancy of one or both **P** sites. In other words, when both **P(1A)** and **P(1B)** are vacant, the **Fe1** subsite is occupied; and when **P(1A)** or **P(1B)** is occupied, the **Fe2** or **Fe3** subsite is occupied, respectively (Figs. 1 and 2). The occupancies of the **Fe** subsites support a proton-cation repulsion mechanism in that **Fe3** has a higher occupancy than **Fe2**. The **P** sites are located in the faces of the **Al(3)** octahedra, implying that when a **P** site is occupied, its corresponding **Al(3)** site is not; so, since **Al(3B)** is less occupied than **Al(3A)**, **P(1B)** should be more occupied than **P(1A)**. If the proton-cation repulsion concept is correct, the occupancies of **Fe2** and **Fe3** could be used as estimates for the occupancies of **P(1A)** and **P(1B)**, respectively. An estimate of H^+ content could then be made from these occupancies. Using the occupancies of the **Fe** subsites from the low-temperature structure refinement, the number of H^+ ions per formula unit for this staurolite would be between 1.96 and 2.20, depending on whether the **P** sites are occupied when the **Fe** site is vacant. This is an unreasonably low amount of H^+ for staurolite [the lowest H^+ content found by Holdaway et al. (1986a) is 2.68 atoms]. However, the large errors for the **Fe**-subsite occupancies could bring the estimated **P**-site occupancy to as high as 2.80, a very reasonable number. More accurate and precise **Fe**-subsite occupancies would be needed to make reliable estimates of **P**-site occupancies.

If the proton-cation repulsion idea is taken one step further to include next-nearest neighbors of the **Fe** site, a better explanation for both the positional disorder and the crystal-field variations at the **Fe** site can be made. Two factors will affect the crystal-field energy at the **Fe** site. First, if occupancy of the **P** site could affect the energy at the **Fe** site, then occupancy or vacancy of other neighboring sites (**Al(3)**, **U**, **Fe**, and kyanite-layer sites) could have an effect on the energy at the **Fe** site (Fig. 1). Second, the energy at the **Fe** site will depend on the identities of the cations occupying neighboring sites. Thus, the three major Mössbauer doublets can be attributed to the three most probable occupancy distributions around the **Fe** site: Al in both **Al(3A)** and **Al(3B)**, Al in **Al(3A)** and H in **P(1B)**, and H in **P(1A)** and Al in **Al(3B)**. Other occupancy distributions (including vacancies and/or substitution of minor cation species in some sites) are reflected in the Mössbauer spectra by line-broadening of the major doublets.

Positional disorder at the **Fe** site is probably a result of variations in the crystal field, since variations in the crystal field could cause changes in the location of the energetic minimum at the site. The location of the energetic minimum could also depend on the identity of the cation in the **Fe** site; some cations may prefer one subsite over another. Comparison of Mössbauer peak areas with structure-refinement subsite occupancies could determine if this is the case. However, for the present study, the statistical errors would mask any differences between the two types of data. If a random distribution of **Fe**-site cation species is assumed, then Mössbauer and electron-density peaks can be tentatively correlated. On the basis of Mössbauer doublet areas and subsite occupancies alone (Tables 8 and 3), **Fe1** would correlate with doublet B, **Fe2** with doublet A, and **Fe3** with doublet C. Assuming all octahedrally coordinated Fe to be Fe^{3+} would result in a correlation between doublet D and the **Al(3)** sites.

Effects of temperature

The occupancies of the **Fe** subsites, determined from X-ray diffraction data, show essentially no change between room and low temperatures, since the differences are all within the range of the statistical errors, in agreement with the Mössbauer results. An apparent temperature dependence in Mössbauer spectra of staurolite has been noted by other workers (Dowty, 1972; Regnard, 1976; Scorzelli et al., 1976; Varma and Varma, 1986); however, no errors for peak parameters are listed, so the validity of the temperature dependence in these spectra cannot be evaluated. For the present staurolite, the apparent change in relative Mössbauer peak areas with temperature is most likely an artifact produced by the difficulty of separating overlapping peaks. Peak separations could be affected by slight changes with temperature in the electric-field gradient around the Fe-occupied sites, which would cause

slight changes in the positions of the corresponding peaks in the Mössbauer spectra.

Conclusions

1. The Fe distribution for the staurolite of this study, derived from structure-refinement data, is 92% in the **Fe** site, 6% in the **Al(3)** sites, and 2% in the **U** sites. Therefore, the Mössbauer spectra for this staurolite are interpreted as representing 92% of the Fe in tetrahedral coordination and 8% in octahedral coordination.

2. The three resolved Fe^{2+} Mössbauer doublets are attributed to energetically nonequivalent **Fe** sites resulting from variations in the crystal-field energy at the site. Crystal-field variations are attributed to occupancy and vacancy distributions and cation substitutions in the neighborhood of the **Fe** site. Line broadening of the Mössbauer doublets (especially doublet C) is attributed to small unresolved doublets arising from less likely variations in the crystal-field energy at the **Fe** site and to small amounts of octahedrally coordinated Fe^{2+} in the **U** sites.

3. Neither the electron density at the **Fe** site nor the Mössbauer spectra exhibit any definite temperature dependence since all variations with temperature are within the range of statistical errors.

Acknowledgments

This project was done in fulfillment of the thesis requirement for an M.S. degree at Brigham Young University. Financial support was provided by a departmental fellowship and by a research grant from the Associated Students of BYU.

References cited

Bancroft, G.M., Maddock, A.G., and Burns, R.G. (1967) Applications of the Mössbauer effect to silicate mineralogy—I. Iron silicates of known crystal structure. Geochimica et Cosmochimica Acta, 31, 2219–2246.

Batsanov, S.S. (1959) Strukturnaya Refraktometriya. University Press, Moscow (translated in P.P. Sutton, Refractometry and chemical structure, 250 p. Consultants Bureau, New York, 1961).

Bloss, F.D. (1981) The spindle stage: Principles and practice, 340 p. Cambridge University Press, Cambridge, England.

Bringhurst, K.N., and Griffen, D.T. (1986) Staurolite-lusakite series. II. Crystal structure and optical properties of a cobaltoan staurolite. American Mineralogist, 71, 1466–1472.

Cromer, D.T., and Liberman, D. (1970) Relativistic calculation of anomalous scattering factors for X-rays. Journal of Chemical Physics, 53, 1891–1898.

Cromer, D.T., and Mann, J.B. (1968) X-ray scattering factors computed from numerical Hartree-Fock wave functions. Acta Crystallographica, A24, 321–324.

De Coster, M., Pollack, H., and Amelinckx, S. (1963) A study of Mössbauer absorption in iron silicates. Physica Status Solidi, 3, 283–288.

Dickson, B.L., and Smith, G. (1976) Low-temperature optical absorption and Mössbauer spectra of staurolite and spinel. Canadian Mineralogist, 14, 206–215.

Dollase, W.L. (1975) Statistical limitations of Mössbauer spectral fitting. American Mineralogist, 60, 257–264.

Dowty, E. (1972) Site distribution of iron in staurolite. Earth and Planetary Science Letters, 15, 72–74.

Dutrow, B.L., Holdaway, M.J., and Hinton, R.W. (1986) Lithium in staurolites: Its petrologic significance. Contributions to Mineralogy and Petrology, 94, 496–506.

Dzhemats, A.C., and Nikitina, L.P. (1977) Mössbauer spectroscopy of staurolite. Leningrad Universitet Vestnik, Geologiia i Geografiia, 24, 42–46.

Griffen, D.T. (1981) Synthetic Fe/Zn staurolites and the ionic radius of $^{IV}Zn^{2+}$. American Mineralogist, 66, 932–937.

Griffen, D.T., and Ribbe, P.H. (1973) The crystal chemistry of staurolite. American Journal of Science, 273-A, 479–495.

Hanisch, K. (1966) Zur Kenntnis der Kristallstruktur von Staurolith. Neues Jahrbuch für Mineralogie Monatshefte, 362–366.

Hawthorne, F.C. (1983) Quantitative characterization of site-occupancies in minerals. American Mineralogist, 68, 287–306.

Holdaway, M.J., Dutrow, B.L., Borthwick, J., Shore, P., Harmon, R.S., and Hinton, R.W. (1986a) H content of staurolite as determined by H extraction line and ion microprobe. American Mineralogist, 71, 1135–1141.

Holdaway, M.J., Dutrow, B.L., and Shore, P. (1986b) A model for the crystal chemistry of staurolite. American Mineralogist, 71, 1142–1159.

Náray-Szabó, I. (1929) The structure of staurolite. Zeitschrift für Kristallographie, 71, 103–116.

Náray-Szabó, I., and Sasvári, K. (1958) On the structure of staurolite, $HFe_2Al_9Si_4O_{24}$. Acta Crystallographica, 11, 862–865.

Phillips, L.V., and Griffen, D.T. (1986) Staurolite-lusakite series. I. Synthetic Fe-Co staurolites. American Mineralogist, 71, 1461–1465.

Regnard, J.R. (1976) Mössbauer study of natural crystals of staurolite. Journal de Physique, Colloque, 37, C6-797–C6-800.

Schreyer, W., Horrocks, P.C., and Abraham, K. (1984) High-magnesium staurolite in a sapphirine-garnet rock from the Limpopo Belt, Southern Africa. Contributions to Mineralogy and Petrology, 86, 200–207.

Scorzelli, R.B., Baggio-Saitovitch, E., and Danon, J. (1976) Mössbauer spectra and electron exchange in tourmaline and staurolite. Journal de Physique, Colloque, 37, C6-801–C6-805.

Sheldrick, G.M. (1976) SHELX-76: A programme for crystal structure determination. University of Cambridge, Cambridge, England.

Smith, J.V. (1968) The crystal structure of staurolite. American Mineralogist, 53, 1139–1155.

Tagai, T., and Joswig, W. (1985) Untersuchungen der Kationenverteilung im Staurolith durch Neutronenbeugung bei 100K. Neues Jahrbuch für Mineralogie Monatshefte, 97–107.

Takéuchi, Y., Aikawa, N., and Yamamoto, T. (1972) The hydrogen locations and chemical composition of staurolite. Zeitschrift für Kristallographie, 136, 1–22.

Varma, H.V., and Varma, J. (1986) Mössbauer effect study of natural staurolite. Physica Status Solidi A, 97, 275–278.

Walker, N., and Stuart, D. (1983) An empirical method for correcting diffractometer data for absorption effects. Acta Crystallographica, A39, 158–166.

Ward, C.M. (1984a) Magnesium staurolite and green chromian staurolite from Fiordland, New Zealand. American Mineralogist, 69, 531–540.

——— (1984b) Titanium and the color of staurolite. American Mineralogist, 69, 541–545.

Manuscript received June 10, 1988
Manuscript accepted January 11, 1989